

Molecular Barcodes: Information Transmission via Persistent Chemical Tags

Linchen Wang¹, Nariman Farsad², Weisi Guo³, Sebastian Magierowski⁴, and Andrew W. Eckford⁵

^{1,2,4,5}Dept. of Electrical Engineering and Computer Science, York University, Toronto, Ontario, Canada

³School of Engineering, University of Warwick, Coventry, United Kingdom

Emails: {¹linchen, ²nariman, ⁴magiero, ⁵aekford}@eecs.yorku.ca, ³weisi.guo@warwick.ac.uk

Abstract—In molecular communication information is conveyed through chemical signals. In this work, we have considered a novel communication scheme where information is encoded in chemical barcodes, through use of persistent chemical tags. We have assumed that this information is already encoded in the environment, and we have devised a robotic platform for reading the chemical tag. We have performed many experiments to find the optimal encoding scheme and an algorithm for reading and decoding the chemically tagged information. We have demonstrated that chemical tags can be decoded using simple algorithms and inexpensive, off-the-shelf sensors. Finally, we have evaluated and presented the bit error rate performance of our devised algorithm.

Index Terms—Molecular Communication; Chemical Tags; Robot Communication; Chemical Communication; Chemical Barcodes; Chemical Signalling

I. INTRODUCTION

Molecular communication [1] is a new and emerging area of science where chemical signals are used to convey information. In the literature, it is typically assumed that a transmitter releases information molecules into the channel where they are transported to the receiver using diffusion [2]–[4], flow [5]–[7], molecular motors [8]–[10], or bacteria [11]–[13]. More recently it was demonstrated that molecular communication can be applied to macroscale [14], where it was demonstrated that short text messages could be communicated by encoding messages into alcohol concentration [15]. In [16], it was shown that molecular communication can outperform radio-based communication in confined metallic environments, such as ducting systems, that are hostile towards radio propagation.

Inspired by these recent advancements, in this work we consider the challenge faced by rescue robots. In particular, in the case of collapsed buildings (for example due to earthquakes) radio signals do not propagate well through concert and rubble. Therefore, rescue robots that go under the rubble may not be able to communicate with each other. To solve this problem, in this work we propose a novel scheme where robots maintain communication through chemical barcodes. It is assumed that the transmitting robot leaves a bar code in the environment using a persistent chemical (similar to the way dogs leave chemical tags in the environment). The receiver robot can then read the barcode when it enters the same environment.

This work was supported in part by a grant from the Natural Sciences and Engineering Research Council.

Chemical communication between robots was initially inspired from pheromonal communication and olfaction from nature [17]. Generally, previous works in this area can be divided into two main streams: pheromone based communication inspired by nature [18]–[21], and plume or chemical tracking robots [22]–[27]. In pheromone based robot communication, the transmitter robot releases infochemical to send a message to the receiver robot. The messages are typically very short and contain little information. In plume and chemical tracking, robots follow a chemical plume (e.g. toxic chemical) to find the source of the plume, or robots follow chemical trails set in place using persistent chemicals. Our work is completely novel and to the best of our knowledge no previous work has considered robot communication through chemical tags.

Our goal in this work is to devise a platform that demonstrates the feasibility of communication through chemical tags. To achieve this goal we first design and build a platform for reading chemical barcodes. We assume that chemical tags are binary coded where a 1 is represented by the presence of a chemical drop and a zero is represented by the absence of a chemical drop in the barcode. We then design experiments to test our platform and systematically design an algorithm for reading these chemical tags. This is a challenging task since metal oxide sensors that have been used in previous works for detecting chemicals and following chemical trails are typically nonlinear [28]. Through experiments, we show that there is an optimal distance between consecutive drops, there is a optimal wait period between drops.

The rest of this paper is organized as follows. In Section II, we present the design for our platform, and discuss the different components that are used in the implementation. In Section III we discuss the experiments we designed and their results. We present an algorithm for reading the barcodes and discuss its bit error rate performance. Concluding remarks and future works are presented in section IV.

II. SYSTEM DESIGN

Our system design is related to our earlier work in [14]. However, in this paper, our goal is to encode information in a persistent chemical “barcode”, and to design a receiver that can read the message. Thus, our system has three key components: the *sensor*, that detects an alcohol concentration; the *mobile platform*, on which the sensor is mounted, and which passes the sensor over the chemical tag; and the *testing*

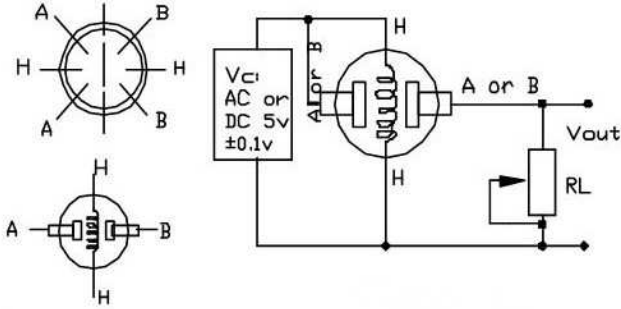


Fig. 1. MQ-3 sensor. Figure from [29].

environment, in which the effectiveness of our system in detecting a chemical signal is evaluated. In the remainder of this section, we describe all three components in detail.

A. Sensor

To detect airborne alcohol concentrations, we use the MQ-3 sensor [29]. This sensor is based on tin oxide (SnO_2) semiconducting sensing layer: after heating to 350°C , the SnO_2 sensor exhibits a drop in electrical resistance in the presence of flammable gases, such as ethanol or propanol [30]. In this work, we use ethanol as the persistent chemical that is used for creating the chemical tags. According to the datasheet the MQ-3 sensor needs to be preheated about 24-48 hours before use. However, we have found that shorter preheat times are also possible. For our experiments, we always keep the sensor connected to the power source, so that it is always ready for use.

Figure 1 gives a sensor schematic: the enveloped MQ-3 has six pins, both A pins and B pins are used to fetch signals, and other two H pins are used for providing heating current. As depicted in Figure 1, the change in sensor resistance in the presence of target gas can be measured using a voltage divider circuit with 0V to +5V output range across a load resistor R_L . Suppose the resistance across the sensor is R_S , which is a function of concentration; then the measured voltage V_{out} is given by

$$V_{\text{out}} = V_{\text{in}} \frac{R_L}{R_S + R_L} = 5 \frac{R_L}{R_S + R_L}. \quad (1)$$

For example, it would return a +5V signal as $R_S \rightarrow 0$ in the presence of alcohol saturation, and 0V as $R_S \rightarrow \infty$ in clean air. The response curves relating R_S to concentration are given in the sensor data sheet [29].

B. Mobile platform

To determine the structure of an alcohol tag, the alcohol sensor needs to pass over the entire tag at close range: thus, it can determine those locations with a significant deposit of alcohol, and those locations where there is none. Thus, we mounted the sensor on a mobile platform, i.e. a robot, which carries the sensor over the tag.

module	amount
Lego MINDSTORM NXT 2.0	1
Arduino microcontroller	1
sensor processing shield	1
TKJ NXT shield	1
NXT motor	2
MQ-3 sensor	1
Micro fan	1

TABLE I
LIST OF COMPONENTS IN THE MOBILE PLATFORM

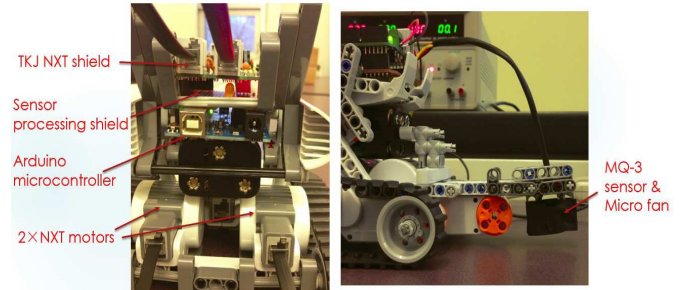


Fig. 2. Design of the robot.

We designed our robot using Lego Mindstorm NXT 2.0, due to its ease of use and reasonable cost. Robot components are illustrated in Figure 2. The robot's processing and control architecture is based on the Arduino system, which is equipped with an NXT shield (to control the robot's movement) and a sensor processing shield (connected to the alcohol sensor). The robot would normally be powered by 6 AA batteries, but we found the weight of these batteries had a significant impact on its maneuverability. Thus, the robot was powered via an external DC power supply, connected to the robot via wire.

As depicted in Figure 2, the alcohol sensor was mounted on the front of the robot, facing downward, so as to be as close as possible to the chemical tag on the ground. Moreover, we packaged the sensor together with a "micro fan", of the type that might be used to cool electronic components. In our case, the fan is used to "sniff" the chemical tag, moving air with a high concentration of alcohol past the sensor; this dramatically improves the performance of the sensor.

A component list for the robot is given in Table I.

C. Testing environment

Figure 3 illustrates the design for reading an alcohol tag. In this work, we assume that the chemical barcodes are in a straight line. Therefore, the robot is constrained by plastic guides, with a ruler to ensure correct placement of the alcohol message. For simplicity, information is encoded by *on-off keying*: a bit $x \in \{0, 1\}$ is transmitted either with a dot of alcohol ($x = 1$) or no alcohol ($x = 0$), with a distance of a few centimetres between drops. Experiments related to inter-dot spacing are described in the next section.

The sensor is located about 1.5 cm above the table, 8 cm from broadside of the robot and 6 cm from front of track of the robot: since we want robot to read alcohol information by

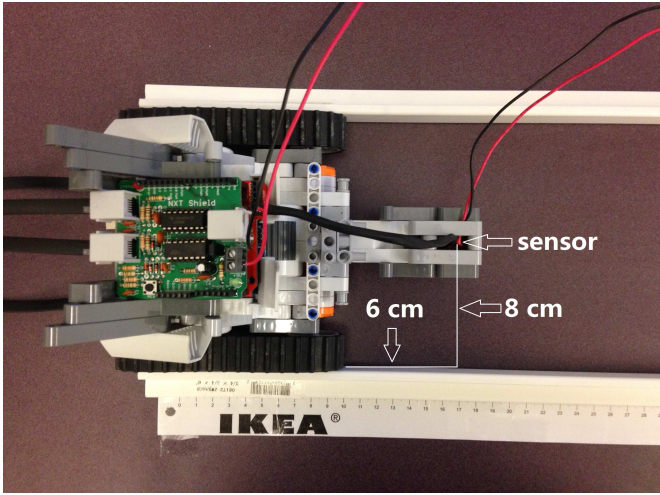


Fig. 3. Design for alcohol reading

passing exactly over the alcohol dots, we would leave the dots under the path of the sensor. A “dot of alcohol” consists of either one or two drops deposited at the required spot, each drop measuring roughly 0.02 ml, measured out by a medicine dropper.

The speed of travel of the robot is roughly 16 cm/s, “half speed” for the robot, though the robot does not read the tag in one continuous motion, but can stop and wait after detecting a drop. Experiments related to the robot’s tag-reading behaviour are described in the next section.

III. EXPERIMENTS AND RESULTS

Our experiments are divided into two parts: tests of strategies to avoid sensor saturation, and tests of optimal encoding strategies and decoding algorithms.

A. Strategies to avoid sensor saturation

In Section II, we described our system design, including a micro fan to force alcohol-concentrated air past the sensor. In this section, we consider reading strategies to maximize the sensor’s ability to detect an alcohol drop. In particular, these experiments show that *saturation* of the sensor is a problem to be avoided.

In this series of experiments:

- Each alcohol dot consists of one drop of alcohol from the medicine dropper;
- There are four dots, with 10 cm spacing between dots; and
- Three runs are completed for each experiment.

Two experiments are performed. In the first experiment, the sensor pauses for 5 s *directly over* the alcohol dot; in the second experiment, the sensor pauses for 5 s *at the midpoint* between alcohol dots (i.e., 5 cm from each).

Measurements for the experiments are given in Fig. 4, where the top plots are the case when the sensor pauses on top of the drop and the bottom plots are the case when the sensor pauses at the midpoint between drops. In each experiment,

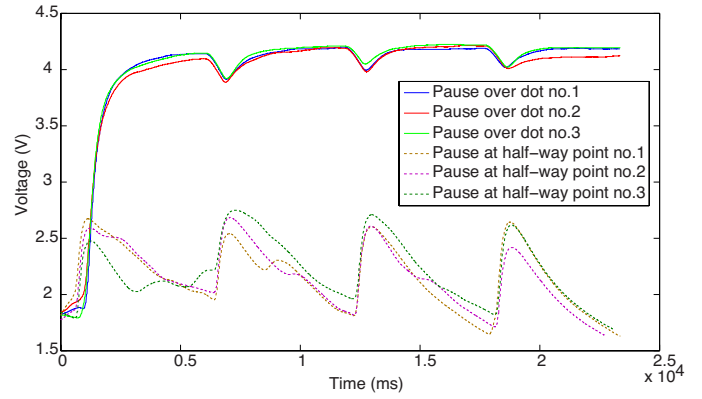


Fig. 4. Sensor measurements for the cases when the sensor pauses on top of the drops (top plots), and the case when the sensor pauses at the midpoint between drops (bottom plots). The duration of pause is 5 seconds for both cases, the distance between the drops is 10 cm, and there are 4 drops.

four voltage maxima are seen, corresponding to the four concentration maxima as the sensor passes over the dots. We see the difference between the maximum and minimum voltage measurement is much *lower*, when the sensor pauses directly over the drop: roughly 0.2 V compared to 0.9 V when the sensor pauses between drops. This is counterintuitive, as one would expect the strongest alcohol signal in this case. However, pausing over the dot causes the sensor to saturate: in the top plots in Fig. 4, the average voltage level of roughly 4 V is close to the power supply voltage of 5 V (i.e., the maximum possible). However, pausing between dots leads to an average voltage level closer to the middle of the possible range. Thus, the strategy of pausing between dots is effective at preventing saturation, while the sensor is still sensitive enough to detect the dot.

In all subsequent experiments, we adopted the approach, where the robot paused for several seconds where no dot was located (at the midpoint between dots), in order to prevent saturation.

B. Symbol detection algorithm

As noted in an earlier section, we use on-off keying to transmit information: a drop of alcohol represents “1”, and no drop represents “0”. Throughout this section, for convenience in our experiments, we use one of two 25-bit sequences to test our system:

$$\mathbf{x} = [1, 0, 1, 1, 0, 1, 1, 0, 1, 1, 0, 1, 1, 0, 1, 1, 0, 0, 1, 0, 1, 1, 0, 0, 1, 1] \quad (2)$$

and its bitwise complement,

$$\bar{\mathbf{x}} = [0, 1, 0, 0, 1, 0, 0, 1, 0, 0, 1, 0, 0, 1, 0, 1, 1, 0, 1, 0, 0, 1, 1, 0, 0, 0] \quad (3)$$

A significant issue with our system is that the sensitivity of the sensor changes over time with use. For example, consider an experiment using the sequence \mathbf{x} , shown in Fig. 5. This figure indicates that the average level of the signal, as well

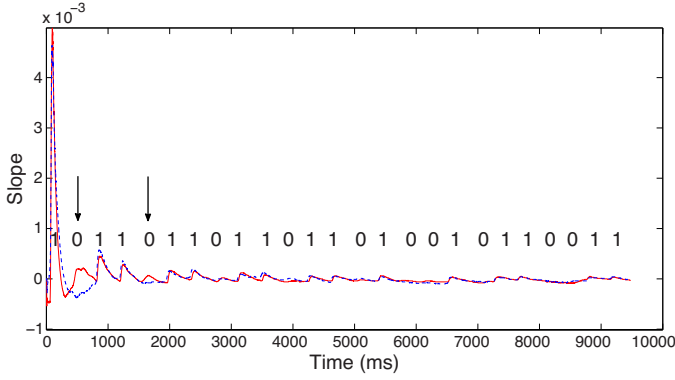


Fig. 5. The slope, ΔV , for the sequence \mathbf{x} .

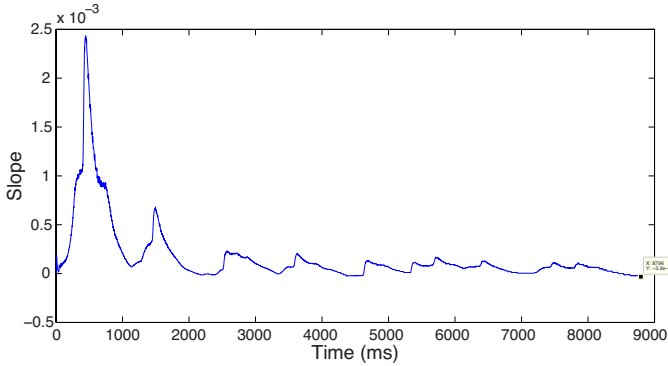


Fig. 6. The slope, ΔV , for the sequence $\bar{\mathbf{x}}$.

as its sensitivity, change significantly from the start of the bit sequence to the end.

Similar issues were encountered in our previous work [14], in which we relied on the rate of change, or “slope” of the voltage to eliminate the effect of the average level of the signal. In particular, if $V(t)$ represents the time measured at time t , and Δt is the time difference between consecutive voltage measurements, we calculate

$$\Delta V(t) = \frac{V(t) - V(t - \Delta t)}{\Delta t}. \quad (4)$$

We refer to $\Delta V(t)$ as the *slope* of the signal. In this work, Δt is 50 ms, which was proved to be optimal through experimentation.

The quantity $\Delta V(t)$ is depicted for the signal $\bar{\mathbf{x}}$ in Figure 6. In this figure, the average $\Delta V(t)$ is now zero (eliminating the issue of changing level), but the declining sensitivity of the sensor is clearly seen: the symbols 0 and 1 can be distinguished from adjacent, different symbols, but over time the change in slope becomes smaller.

Our approach is to detect symbols using a threshold that changes with time, $\text{th}(t)$. That is, the detected bit \hat{b} is given by

$$\hat{b} = \begin{cases} 0, & \Delta V(t) < \text{th}(t) \\ 1, & \Delta V(t) \geq \text{th}(t) \end{cases}. \quad (5)$$

The changing threshold $\text{th}(t)$ is dependent on the instanta-

neous sensitivity of the sensor, which in turn is dependent on the transmitted information sequence. In the absence of a theoretical characterization of the sensor (which is forthcoming in future work), $\text{th}(t)$ must be characterized experimentally. In full generality, we should run several experiments each for all possible input sequences in $\{0, 1\}^n$, though the complexity of these experiments would quickly become prohibitive. Therefore, we obtain a suboptimal $\text{th}(t)$ as follows:

- 1) Perform 5 experiments with \mathbf{x} . Let $V_{\mathbf{x},i}(t)$ represent the voltage readings for the i th experiment as a function of time.
- 2) Perform 5 experiments with $\bar{\mathbf{x}}$. Let $V_{\bar{\mathbf{x}},j}(t)$ represent the voltage readings for the j th experiment as a function of time.
- 3) If $\max_{j \in \{1, \dots, 5\}} V_{\bar{\mathbf{x}},j}(t) < \min_{i \in \{1, \dots, 5\}} V_{\mathbf{x},i}(t)$, then

$$\text{th}(t) = \frac{1}{2} \left(\max_{j \in \{1, \dots, 5\}} V_{\bar{\mathbf{x}},j}(t) + \min_{i \in \{1, \dots, 5\}} V_{\mathbf{x},i}(t) \right). \quad (6)$$

(This should be the case if $\mathbf{x}_k = 1$.) If $\max_{i \in \{1, \dots, 5\}} V_{\mathbf{x},i}(t) < \min_{j \in \{1, \dots, 5\}} V_{\bar{\mathbf{x}},j}(t)$, then

$$\text{th}(t) = \frac{1}{2} \left(\max_{i \in \{1, \dots, 5\}} V_{\mathbf{x},i}(t) + \min_{j \in \{1, \dots, 5\}} V_{\bar{\mathbf{x}},j}(t) \right). \quad (7)$$

(This should be the case if $\mathbf{x}_k = 0$.) Otherwise, if neither of the above conditions hold, then $\text{th}(t)$ is the average of all $V_{\mathbf{x},i}(t)$ and $V_{\bar{\mathbf{x}},j}(t)$.

Equations (6)-(7) are analogous to finding a threshold using an eye diagram in conventional communication systems.

We test this scheme, by using both \mathbf{x} and $\bar{\mathbf{x}}$ sequences and the solution above. The experiment corresponding to each sequence is repeated 6 times. We observed 13 bit error in a total of 12 experiments (300 bits total), and therefore, the estimated probability of bit error is 4.3%.

C. Drop separation and pause time

In this section, we consider the optimization of two key system parameters: the *drop separation*, or the shortest possible distance between adjacent dots; and the *pause time*, or the length of time that is spent between dots in the saturation-avoidance strategy.

As before the symbols are encoded by each dot (on-off-keying), and robot would pause at the midpoint between drops according to a prespecified delay time. To find out the optimal distance between dots and the optimal delay (pause) time, we chose a 20 bit sequence (the first 20 bits of \mathbf{x}) to test the error rate. The bit detection scheme in the previous section was used, and each experiment was repeated 5 times to for calculating the average error rate.

Fig. 7 illustrates the error rate for 6 cm, 8 cm, 10 cm, and 12 cm. The pause duration is 5 seconds for all distances. The error rate drops when the distance increases and then reaches an error floor. A short distance between the dots seems to cause a high error rate. This is in part because the robot can not stop at the midpoint accurately for the delay pause. For example, it might stop too close to the next dot; moreover, there is an inter-symbol interference when the dots are very

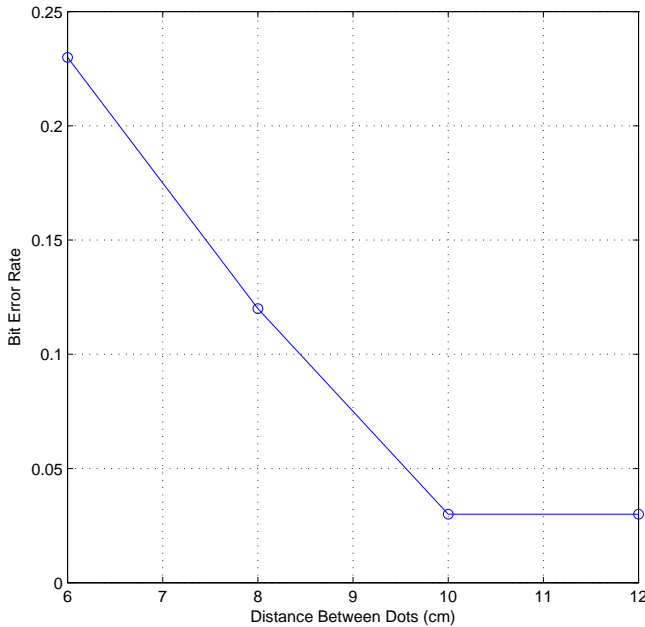


Fig. 7. Bit error rate as a function of separation distance between dots. The pause duration is 5 seconds.

closely spaced. From Fig. 7, it is evident that the optimal distance between drops is 10 cm.

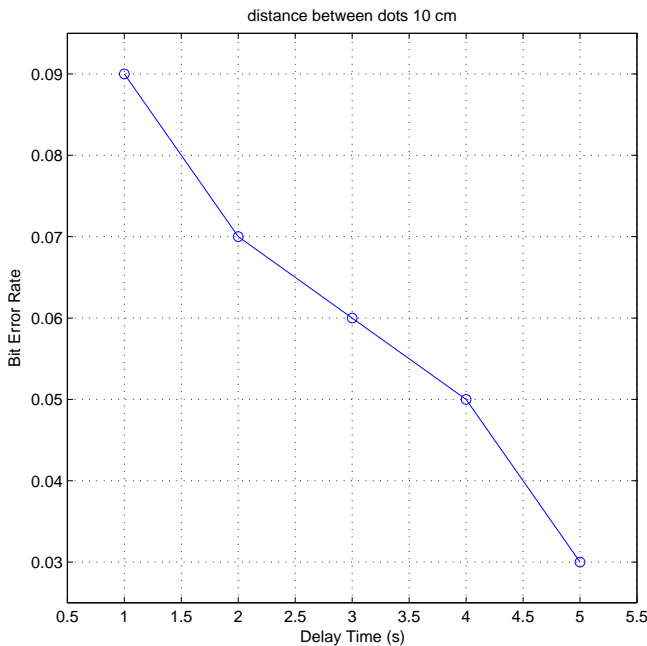


Fig. 8. Bit error rate as a function of delay (pause) time at the midpoint between dots. The distance between the dots is 10 cm.

Fig. 8 shows how the error rate changes as the pause time changes from 1 to 5 seconds. The separation distance is 10 cm for all pause durations. The error rate decrease as the delay time increase since robot has more time to recover. In our initial experiments, delay of 7 seconds did not improve the

error rate. Therefore, we did not complete those experiments and it seems that 5 seconds is the optimal delay duration. An interesting observation from these experiments was that the dominant source of error, when the pause duration was between 3 to 4 seconds, was misdetection of a zero that followed a one in the sequence (e.g. the first two 0s with the arrow on top in the red solid plot of Fig. 5). Besides this source of error, there are almost no other sources of error for delay durations of 3 to 4 seconds. This is because after detecting a dot, 3 to 4 seconds is not enough recovery time for the sensor. Therefore, to improve our detection algorithm, we consider a variable delay (pause) duration D_k for the $k = 1, 2, \dots$ drop positions given by

$$D_k = \begin{cases} 3, & \hat{b}_k = 0 \\ 5, & \hat{b}_k = 1 \end{cases}, \quad (8)$$

where \hat{b}_k is the bit that is detected during the first 3 seconds of the pause duration. Therefore, if a bit one is detected the sensor will pause for an extra 2 seconds to help the sensor recover. This speeds up the barcode decoding algorithm.

IV. CONCLUSION

In this paper we built a platform for decoding messages encoded in chemical barcodes. We used alcohol as the persistent chemical used to create the chemical tags. We then built a robotic platform equipped with MQ-3 metal oxide sensor for detecting the barcodes. We then designed experiments to evaluate the system tolerance and designed a decoding algorithm based on the results. The bit error rate performance of the system was then evaluated, and it was shown that there is an optimal separation distance between drops, and an optimal pause duration after reading each drop.

Detection of persistent chemical tags is a promising future direction for molecular communication, as it provides functionality that few other contemporary communication techniques allow: namely, leaving a message that can be read later, where the presence of a message may not be detected at a distance (even if the message itself can only be read at close range). As a result, this form of molecular communication may be useful at all length scales, not merely at the nanoscale. This work should be considered a proof-of-concept, and future work will optimize system parameters, and produce theoretical analysis to better understand this communication scheme.

REFERENCES

- [1] T. Nakano, A. W. Eckford, and T. Haraguchi, *Molecular communication*. Cambridge University Press, 2013.
- [2] M. Pierobon and I. F. Akyildiz, "Diffusion-based noise analysis for molecular communication in nanonetworks," *IEEE Transactions on Signal Processing*, vol. 59, no. 6, pp. 2532–2547, 2011.
- [3] M. S. Kuran, H. B. Yilmaz, T. Tugcu, and I. F. Akyildiz, "Interference effects on modulation techniques in diffusion based nanonetworks," *Nano Communication Networks*, vol. 3, pp. 65–73, Mar. 2012.
- [4] H. B. Yilmaz, A. C. Heren, T. Tugcu, and C.-B. Chae, "Three-dimensional channel characteristics for molecular communications with an absorbing receiver," *IEEE Communications Letters*, vol. 18, no. 6, pp. 929–932, 2014.

- [5] K. V. Srinivas, A. Eckford, and R. Adve, "Molecular communication in fluid media: The additive inverse gaussian noise channel," *IEEE Transactions on Information Theory*, vol. 58, no. 7, pp. 4678–4692, 2012.
- [6] H. ShahMohammadian, G. G. Messier, and S. Magierowski, "Nanomachine molecular communication over a moving propagation medium," *Nano Communication Networks*, vol. 4, no. 3, pp. 142–153, 2013.
- [7] A. Noel, K. Cheung, and R. Schober, "Optimal receiver design for diffusive molecular communication with flow and additive noise," *IEEE Transactions on NanoBioscience*, vol. 13, pp. 350–362, Sept 2014.
- [8] A. Enomoto, M. J. Moore, T. Suda, and K. Oiwa, "Design of self-organizing microtubule networks for molecular communication," *Nano Communication Networks*, vol. 2, no. 1, pp. 16–24, 2011.
- [9] N. Farsad, A. Eckford, S. Hiyama, and Y. Moritani, "On-Chip Molecular Communication: Analysis and Design," *IEEE Transactions on NanoBioscience*, 2012.
- [10] N. Farsad, A. Eckford, and S. Hiyama, "A markov chain channel model for active transport molecular communication," *IEEE Transactions on Signal Processing*, vol. 62, pp. 2424–2436, May 2014.
- [11] M. Gregori, I. Llatser, A. Cabellos-Aparicio, and E. Alarcn, "Physical channel characterization for medium-range nanonetworks using flagellated bacteria," *Computer Networks*, vol. 55, no. 3, pp. 779–791, 2011.
- [12] P. Lio and S. Balasubramaniam, "Opportunistic routing through conjugation in bacteria communication nanonetwork," *Nano Communication Networks*, vol. 3, no. 1, pp. 36–45, 2012.
- [13] S. Balasubramaniam and P. Lio, "Multi-hop conjugation based bacteria nanonetworks," *IEEE Transactions on NanoBioscience*, vol. 12, pp. 47–59, March 2013.
- [14] N. Farsad, W. Guo, and A. W. Eckford, "Tabletop molecular communication: Text messages through chemical signals," *PLOS ONE*, vol. 8, p. e82935, Dec 2013.
- [15] N. Farsad, W. Guo, and A. W. Eckford, "Molecular Communication Link," in *IEEE Conference on Computer Communications*, 2014.
- [16] S. Qiu, W. Guo, S. Wang, N. Farsad, and A. Eckford, "A Molecular Communication Link for Monitoring in Confined Environments," in *IEEE Conference on Computer Communications*, 2014.
- [17] R. A. Russell, *Odour detection by mobile robots*. Singapore; River Edge, NJ: World Scientific, 1999.
- [18] Y. Kuwana, S. Nagasawa, I. Shimoyama, and R. Kanzaki, "Synthesis of the pheromone-oriented behaviour of silkworm moths by a mobile robot with moth antennae as pheromone sensors," *Biosensors and Bioelectronics*, vol. 14, no. 2, pp. 195–202, 1999.
- [19] A. H. Purnamadajaja and R. A. Russell, "Pheromone communication in a robot swarm: Necrophoric bee behaviour and its replication," *Robotica*, vol. 23, pp. 731–742, Nov. 2005.
- [20] A. H. Purnamadajaja and R. A. Russell, "Bi-directional pheromone communication between robots," *Robotica*, vol. 28, no. 01, pp. 69–79, 2010.
- [21] M. Cole, Z. Racz, J. Gardner, and T. Pearce, "A novel biomimetic infochemical communication technology: From insects to robots," in *2012 IEEE Sensors*, pp. 1–4, Oct 2012.
- [22] H. Ishida, T. Nakamoto, T. Moriizumi, T. Kikas, and J. Janata, "Plume-tracking robots: A new application of chemical sensors," *The Biological Bulletin*, vol. 200, no. 2, pp. 222–226, 2001.
- [23] S. Larionova, N. Almeida, L. Marques, and A. Almeida, "Olfactory coordinated area coverage," *Autonomous Robots*, vol. 20, no. 3, pp. 251–260, 2006.
- [24] W. Li, J. Farrell, S. Pang, and R. Arrieta, "Moth-inspired chemical plume tracing on an autonomous underwater vehicle," *IEEE Transactions on Robotics*, vol. 22, pp. 292–307, April 2006.
- [25] P. Sousa, L. Marques, and A. de Almeida, "Toward chemical-trail following robots," in *Seventh International Conference on Machine Learning and Applications*, pp. 489–494, Dec 2008.
- [26] A. Ramirez, A. Rodriguez, A. Lopez, D. Bertol, and A. de Albornoz, "Environmental odor perception: an evaluation of aplatform based on labview and the lego nxt," in *ISSNIP Biosignals and Biorobotics Conference*, pp. 1–5, 2010.
- [27] A. de Albornoz, A. Rodriguez, A. Lopez, and A. Ramirez, "A microcontroller-based mobile robotic platform for odor detection," in *ISSNIP Biosignals and Biorobotics Conference*, pp. 1–6, Jan 2012.
- [28] N. Farsad, N.-R. Kim, A. W. Eckford, and C.-B. Chae, "Channel and Noise Models for Nonlinear Molecular Communication Systems," *IEEE Journal on Selected Areas of Communications*, 2014.
- [29] Zhengzhou Winsen Electronics Technology Co. Ltd. of China, *MQ3*. Online: <https://www.sparkfun.com/datasheets/Sensors/MQ-3.pdf>.
- [30] J. Watson, "The tin oxide gas sensor and its applications," *Sensors and Actuators*, vol. 5, no. 1, pp. 29–42, 1984.